Aging Cell (2009) **8**, pp128–139 Doi: 10.1111/j.1474-9726.2009.00457.x

A free radical-generating system induces the cholesterol biosynthesis pathway: a role in Alzheimer's disease

María Recuero,[1,2†] M[a] Carmen Vicente,[1†] Ana Martínez-García,[1,2] María C. Ramos,[3] Pedro Carmona-Saez,[4] Isabel Sastre,[1,2] Jesús Aldudo,[1,2] Elisabet Vilella,[5] Ana Frank,[2,6] María J. Bullido[1,2] and Fernando Valdivieso[1,2]

[1]Departamento de Biología Molecular and Centro de Biología Molecular Severo Ochoa (U.A.M.-C.S.I.C.), Cantoblanco, 28049 Madrid, Spain
[2]Centro de Investigación en Red de Enfermedades Neurodegenerativas (CIBERNED), Spain
[3]Neuron Biopharma, 18100 Armilla (Granada), Spain
[4]Integromics S.L., Cantoblanco, 28049 Madrid, Spain
[5]Hospital Psiquiatric Universitari Institut Pere Mata, IISPV, Universitat Rovira I Virgili, 43201 Reus (Tarragona), Spain
[6]Servicio de Neurología, Hospital Universitario La Paz (UAM), 28034 Madrid, Spain

Summary

Oxidative stress, which plays a critical role in the pathogenesis of neurodegenerative diseases such as Alzheimer's disease (AD), is intimately linked to aging – the best established risk factor for AD. Studies in neuronal cells subjected to oxidative stress, mimicking the situation in AD brains, are therefore of great interest. This paper reports that, in human neuronal cells, oxidative stress induced by the free radical-generating xanthine/xanthine oxidase (X-XOD) system leads to apoptotic cell death. Microarray analyses showed a potent activation of the cholesterol biosynthesis pathway following reductions in the cell cholesterol synthesis caused by the X-XOD treatment; furthermore, the apoptosis was reduced by inhibiting 3-hydroxy-3-methylglutaryl-coenzyme A reductase (*HMGCR*) expression with an interfering RNA. The potential importance of this mechanism in AD was investigated by genetic association, and it was found that *HMGCR*, a key gene in cholesterol metabolism and among those most strongly upregulated, was associated with AD risk. In summary, this work presents a human cell model prepared to mimic the effect of oxidative stress in neurons that might be useful in clarifying the mechanism involved in free radical-induced neurodegeneration. Gene expression analysis followed by genetic association studies indicates a possible link among oxidative stress, cholesterol metabolism and AD.

Key words: oxidative stress, cell injury, neurodegeneration, cholesterol, *HMGCR*, genetic association, Alzheimer's disease.

Introduction

Alzheimer's disease (AD) is characterized pathologically by the presence of two hallmark lesions in the brain: extracellular senile plaques (SP) and intraneuronal neurofibrillary tangles (NFT). SP contain amyloid-β (Aβ) peptide, mainly Aβ (1-42), whereas NFT are composed mainly of the microtubule-associated protein τ, present as paired helical filaments. However, SP and NFT may be more an effect than the cause of the disease (Lee *et al*., 2007). Indeed, a theory currently gaining favour suggests that the deposition of SP and NFT is a response of the brain to counteract the effects of a number of toxic molecules (Lee *et al*., 2007).

Oxidative stress is thought to contribute to neuronal injury in acute pathological states of the brain, including transient ischemia, trauma and a number of degenerative diseases of the central nervous system, including AD (Andersen, 2004; Moreira *et al*., 2005; Nunomura *et al*., 2006). The exposure of biological systems to oxidative stress leads to age-dependent increases in the cellular levels of oxidatively modified proteins, lipids and nucleic acids. This subsequently predisposes the organism to the development of well-recognized, age-related disorders that cause impaired cognitive function and reduced metabolic integrity (Stadtman, 2002). The best established risk factor for AD is age, but a large number of studies record oxidative stress in the brains and peripheral tissues of patients with AD, as well as in animal models of the disease (Gibson & Huang, 2005).

Oxidative stress is defined as the imbalance between biochemical processes leading to the production of reactive oxygen species (ROS) and those responsible for their removal – the so-called antioxidant cascade (Harman, 1981). Thus, the ability of cells to detoxify ROS is crucial for homeostasis and survival. Indeed, free radical production has been implicated in the development of cancer, in the progression of neurodegenerative diseases and in the aging process itself (Hayes *et al*., 1999). Previous studies have shown that oxidative damage is the earliest event in AD (Nunomura *et al*., 2001) and that oxidatively damaged RNA is mainly found in the cytoplasm (Nunomura *et al*., 1999). This is a prominent feature of vulnerable neurons in AD, and is consistent with the hypothesis that mitochondria are a major source of the ROS known to cause oxidative damage in this disease.

Several membrane functions in different subcellular compartments have been shown affected by agents that cause oxidative

Correspondence
María J. Bullido, PhD, Tel.: +34 91 1964567; fax: +34 91 1964420; e-mail: mjbullido@cbm.uam.es
[†]These authors contributed equally to this work.

Accepted for publication *1 January 2009*

Aging Cell

damage. There is accumulating evidence to suggest that protein folding, endoplasmic reticulum (ER) stress and the production of ROS are intimately intertwined (Malhotra & Kaufman, 2007). While the causative effects of neurodegenerative diseases are still under investigation, it is clear that alterations in protein folding and redox homeostasis are involved (Forman *et al*., 2003; Yankner *et al*., 2008). What is less clear is the nature of the mechanism linking oxidative stress and cell death. Studies of the possible cellular alterations take place in the presence of oxidative stress are therefore of great interest.

The present paper reports a human neuroblastoma SK-N-MC cell model that involves cells being driven to apoptotic death by oxidative stress induced by a free radical-generating system (Fatokun *et al*., 2007). To elucidate the molecular processes involved, microarray analysis was used to study the overall gene expression profile prior to and during neuronal apoptosis induced by the xanthine/xanthine oxidase (X-XOD) system. Gene expression profiling through such analysis could provide useful starting points for more in-depth investigations designed to explore the molecular changes that occur after X-XOD treatment, and in the search for signature pathways leading to X-XOD-induced neuronal cell death. Interestingly, the present results indicate that oxidative stress induces cholesterol biosynthesis.

Studies involving cell and animal models of neurodegeneration, which are based both on mutations causing monogenic AD and on genes associated with sporadic AD, support the AD–cholesterol homeostasis link. Epidemiological studies have shown that individuals with elevated serum cholesterol levels are more susceptible to this neurodegenerative dementia (Jarvik *et al*., 1994; Tan *et al*., 2003; Ledesma & Dotti, 2006). Further, a microarray study by Blalock *et al*. (2004) showed the expression of a large number of genes related to cholesterol and lipoprotein function to be modified in the AD hippocampus.

Familial AD is caused by mutations in the genes *APP*, *PSEN1* or *PSEN2*; this affects *APP* processing and the generation of neurotoxic β-amyloid peptides (see http://www.alzforum.org for debates/). Such mutations, however, are also likely to affect cholesterol and lipoprotein function (Wirths *et al*., 2006). In addition, AD in 60% of people over the age of 65 years, and in 92% of those below this age, is related to *APOE* variants (Rubinsztein & Easton, 1999). Interestingly, *APOE4*, the allele with the strongest genetic risk factor for sporadic AD, is also associated with high cholesterol levels (Gomez-Isla *et al*., 1996).

Genetic association is a useful tool for investigating the possible importance of candidate molecules or biological processes (obtained from models) in disease. The present work investigates the association of polymorphisms in *HMGCR* and *HMGCS1* with AD because these were among the genes most responsive to the oxidative stress induced, and because they (especially *HMGCR*) represent important control points in cholesterol biosynthesis. The data suggest that cholesterol synthesis is probably involved in AD neurodegeneration since polymorphism in *HMGCR* was found to be associated with AD risk.

Results

X-XOD induces cell death in SK-N-MC cells: cell injury and increased cytosolic calcium levels

The first objective was to characterize the response of the cells to oxidative stress induced by X-XOD treatment (White *et al*., 1998). The viability of the cultures was determined using the MTT assay. This showed cell viability was reduced in a dose-dependent manner at concentrations of > 50 mU mL^{-1} xanthine oxidase (Supplementary Fig. S1A). Thus, the exposure of the cells to oxidative stress resulted in cell injury.

Cytosolic free calcium plays a number of crucial roles in a variety of cell signalling pathways involved in cytoskeleton dynamics, gene regulation and cell proliferation (Ghosh & Greenberg, 1995). For the measurement of cytosolic calcium levels, the cells were loaded with the calcium sensitive dye fluo-4 and incubated with X-XOD at the indicated concentrations (Supplementary Fig. S1B). Oxidative stress treatment produced a significant increase in cytosolic calcium, which was dependent on the X-XOD concentration. The time course of the response showed maximum fluorescence levels was approached within 10 s. Pre-incubation with TMB-8 attenuated the increase in cytosolic calcium after X-XOD treatment by 40% (data not shown), suggesting that this increase was partly due to the mobilization of calcium from the endoplasmic reticulum. The results, therefore, establish that oxidative stress induced with X-XOD leads to loss of neuronal viability and to increased cytosolic calcium levels.

X-XOD-induced cell death in the SK-N-MC cells is apoptotic

Although further studies are required to determine whether cell death is mediated by increased cytoplasmic calcium, the generation of pathological Ca^{2+} signals may be responsible for cell damage that could result in apoptosis (Hajnoczky *et al*., 2003).

The mitochondrion plays a prominent role in the intrinsic apoptosis pathway, and during mitochondrial dysfunction several essential players in apoptosis, including procaspases, cytochrome *c* and apoptosis-inducing factor, are released into the cytosol (Marques *et al*., 2003). Mitochondrial dysfunction was characterized in the present model by studying cytochrome *c* release.

As shown by the immunofluorescence patterns in Fig. 1(A), cytochrome *c* was compartmentalized in the mitochondria in the control culture; this was more visible when the cells were exposed to MitoTracker before cytochrome *c* staining. However, significant amounts of cytochrome *c* were released into the cytosol after 48 h of treatment with X-XOD.

We also studied caspase 3 activation and the degradation of the caspase substrate, PARP (Fig. 1B,C). Flow cytometry was used to follow caspase 3 activation via anti-cleaved caspase 3 labelling. This was performed to determine the time course of caspase 3-like activity induction by X-XOD. Caspase 3-like activity increased following 48 h of X-XOD treatment. However, caspase 3-like activity was partially recovered in the presence of the

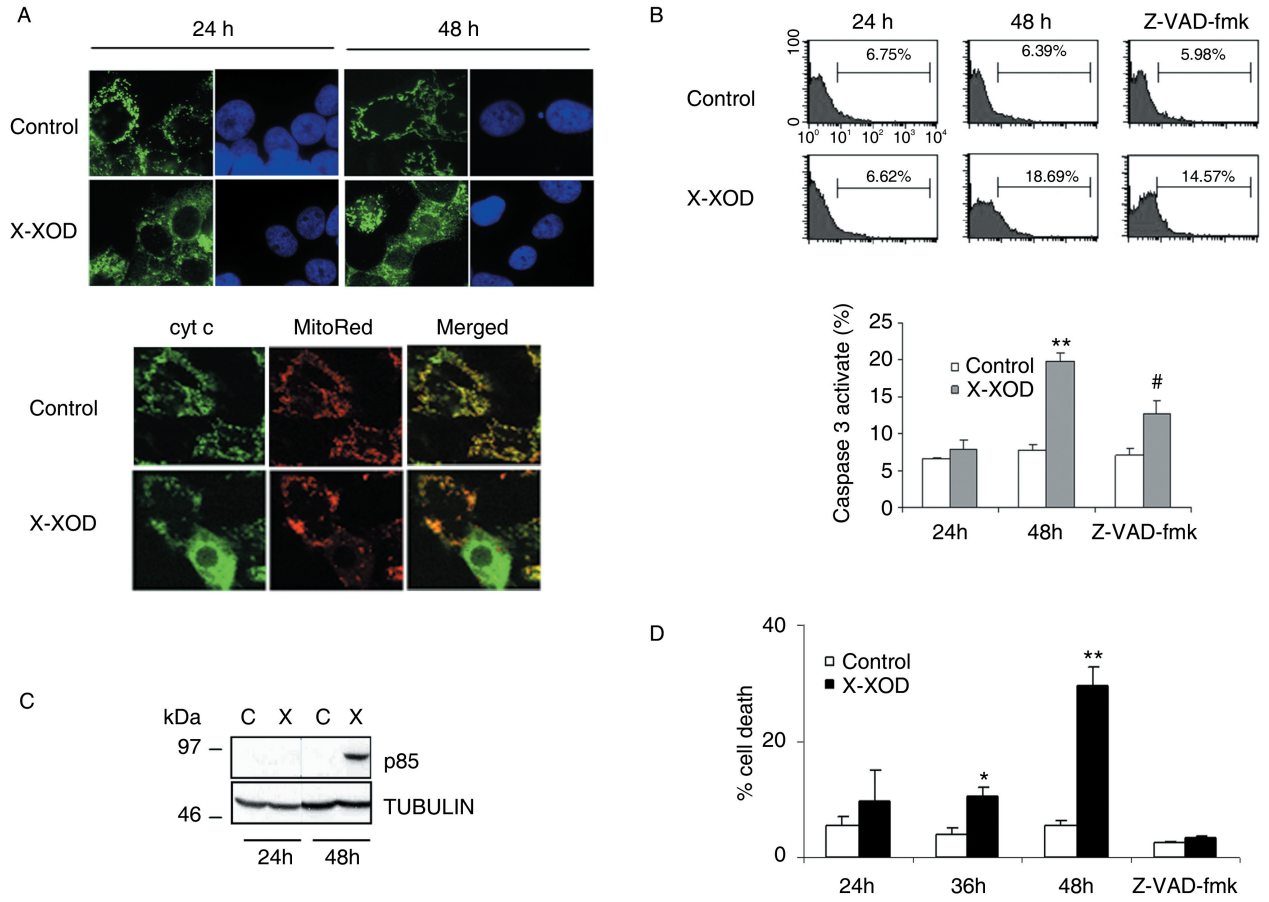

Fig. 1 Cytochrome c release, activation of caspase 3, PARP p85 fragment and quantification of apoptotic cell death induced by the X-XOD system. SK-N-MC cells were submitted to 10 μM xanthine/50 mU mL^{-1} xanthine oxidase (X-XOD), for the indicated incubation time (h). (A) Cytochrome *c* release from mitochondria induced by oxidative stress. The upper panel shows the immunofluorescent labelling by the cytochrome *c* antibody (green) combined with DAPI staining of nuclear morphology (blue) of cells subjected to oxidative stress. In the lower panel, cells treated for 48 h were loaded with MitoTracker® to stain the mitochondria, and then fixed and processed for immunofluorescence analysis. Two images of the same field stained with MitoTracker® (MitoRed: red) and with the cytochrome *c* antibody (cyt *c*: green) are shown; merged images were generated by overlaying using Adobe Photoshop 7.0. For each cell culture, six fields of three independent cultures were analysed. (B) Activation of caspase 3 by oxidative stress. Cells were subjected to X-XOD treatment with or without the caspase inhibitor Z-VAD-fmk (for 48 h). The samples were stained with anti-cleaved caspase 3 antibody and analysed by flow cytometry. The percentage of cells showing active caspase 3 is indicated in each histogram; the data correspond to one representative experiment. The percentage of cells showing active caspase 3 is given as the mean ± SEM of values for three independent experiments. Bars correspond to the standard error [$**P < 0.01$ compared to controls (Student *t*-test); $\#P < 0.05$ compared to 48 h-treated cells]. (C) Western blot showing the quantity of the PARP p85 fragment for the indicated incubation time (h). Representative gels are shown; the bands correspond to the p85 protein. In the lower panel the band corresponds to α-tubulin. (D) Quantification of apoptotic cell death due to oxidative stress. Cells were treated with X-XOD for the indicated incubation time (h), with or without the caspase inhibitor Z-VAD-fmk (for 48 h). Apoptosis was assessed by propidium iodide staining and analysed by flow cytometry. Percentage cell death is given as the mean ± SEM of three independent experiments. The Student *t*-test revealed significant differences compared to controls ($**P < 0.01$ and $*P < 0.05$).

cell-permeable pan-caspase inhibitor Z-VAD-fmk. The activation of caspase 3 was confirmed by analysing the degradation of the caspase substrate, PARP (Hengartner, 2000). In Western blotting, the PARP p85 fragment (Fig. 1C) resulting from caspase 3 cleavage of the 116 kDa intact molecule, revealed PARP to be degraded by X-XOD treatment after 48 h.

The data show that X-XOD generates an apoptotic signal that leads to caspase activity. Further, the results suggest that the oxidative stress caused by X-XOD triggers a specific apoptotic cascade involving caspase 3 in a cytochrome *c*-dependent manner.

Apoptosis was quantified by flow cytometry after propidium iodide staining of the cells (Fig. 1D). When the cells were exposed to X-XOD, the percentage of apoptotic cells increased (36 h: 10.65 ± 1.26%, 48 h: 29.59 ± 3.05%). No apoptosis was seen at 24 h. Further, the caspase inhibitor Z-VAD-fmk significantly reduced apoptotic levels.

Differential gene expression after X-XOD treatment suggests the strong induction of cholesterol biosynthesis

Genes differently expressed in X-XOD-treated and control cells were identified using microarrays and employing the RankProduct method. Using an FDR cut-off of 0.05 and a fold change of two or higher, 211 genes were found to be significantly overexpressed and 83 significantly repressed in the treated cells after 18 h

Table 1 Genes of the cholesterol biosynthesis pathway modulated by X-XOD in SK-N-MC neuroblastoma cells

Probe ID*	Entrez ID†	Gene Symbol	Fold incr‡	FDR§	GO_Biological_process¶
216424	3157	*HMGCS1*	2.2	0.0000	Lipid metabolismlcholesterol biosynthesislacetyl-CoA metabolism
197774	3156	*HMGCR*	1.8	0.0008	Lipid metabolismlgonad developmentlcholesterol biosynthesislgerm cell migration
230255	4597	*MVD*	1.6	0.0008	Isoprenoid biosynthesislphosphorylationlcholesterol biosynthesis
122603	3422	*IDI1*	1.6	0.0019	Carotenoid biosynthesislisoprenoid biosynthesislcholesterol biosynthesis
229668	2224	*FDPS*	1.4	0.0053	Isoprenoid biosynthesislcholesterol biosynthesis
148144	2222	*FDFT1*	1.1	0.0296	Isoprenoid biosynthesislcholesterol biosynthesis
136461	4598	*MVK*	1.1	0.0433	Metabolismlisoprenoid biosynthesislprotein amino acid phosphorylationlcholesterol biosynthesis

Microarray probe identification (*), the code (†) and official symbol of the gene in the Entrez NCBI database, the mean fold change in X-XOD treated vs. untreated cells, expressed as $\log_2$ (‡) with the significance (false discovery rate, FDR) value (§), and the biological processes associated to each gene according to the GO annotations provided in the array annotation file from Applied Biosystems (¶).

compared to controls. Table 1 shows the genes coding for enzymes of the cholesterol biosynthesis pathway, and the complete gene list is provided as supplementary table; quantitative RT-PCR was used to verify the expression of 10 genes representative of different functional clusters and overexpression levels (see Supplementary Fig. S2).

Interestingly, a significant enrichment of Gene Ontology (GO) annotations related with cholesterol and lipid metabolism in the list of over-expressed genes was observed (Supplementary table), being 'cholesterol biosynthesis' the annotation that was found most significant in this gene set (FDR < 10^{-13}). Indeed, seven (*HMGCS1*, *HMGCR*, *MVK*, *MVD*, *IDI1*, *FDPS*, *FDFT1*) of the nine genes encoding the enzymes driving the synthesis of squalene from acetyl CoA were overexpressed. Other enzymes involved in cholesterol biosynthesis steps after squalene production were also upregulated, such as 24-dehydrocholesterol reductase (encoded by *DHCR24*).

The group of under-expressed genes contained seven involved in chromatin structure and remodelling (the histones of the H1 family *HIST1H4C*, *HIST1H4D*, *HIST1H4F*, *HIST1H4J*, *HIST1H4K* and *H1F0*); the remaining repressed genes were not significantly clustered to biological processes identified in the GO database.

In summary, the main effect of the X-XOD treatment appears to be the regulation of lipid metabolism, and more specifically an activation of the first rate limiting steps of cholesterol biosynthesis.

X-XOD modulates cholesterol biosynthesis

To determine whether the observed transcriptional activation was related to the deregulation of cholesterol levels, cholesterol biosynthesis was studied by measuring the incorporation of a radiolabel into free cholesterol and cholesteryl esters (CE), using [1–^{14}C] acetate as a lipid precursor. Figure 2 shows the radioactivity incorporated into cholesterol present in the cells (A) or the corresponding culture media (B) at different treatment times. The incorporation of radioactivity into cellular free cholesterol was much higher than into the other cholesterol pools. It can be observed that the incorporation of labelled acetate into cholesterol was significantly reduced in cells treated with X-XOD for 36 h, it approached that seen in control cells after 48 h of treatment, and it was increased two-fold in cells treated for 65 h. This kinetic trend was most evident and significant in the cellular free cholesterol, but was similar to this one in the other pools analysed (cellular CE and culture medium free cholesterol and CE), indicating that the effect of X-XOD on the radiolabel incorporation was actually due to biosynthesis and not to cholesterol transport across cell membranes.

In summary, these results suggest that X-XOD treatment leads to a reduction in cholesterol biosynthesis at early treatment times, followed by a later increase that is at least partly mediated by a transcriptional activation of the key genes in the biosynthesis pathway.

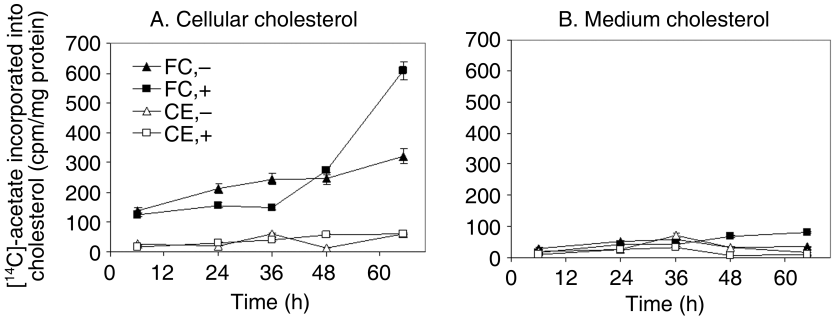

Fig. 2 Biosynthesis of cholesterol (FC) (■, ▲) and cholesteryl esters (CE) (□, △) in SK-N-MC cells treated for the indicated times, with 10 μM xanthine-50 mU mL^{-1} xanthine oxidase (X-XOD) in MEM/10% FBS (+) (■, □) or with vehicle (–) (▲, △). [1–^{14}C]acetate (3.4 mM, 60 Ci mol^{1}) was added 6 h before the end of the treatment period. The incorporation of acetate into cholesterol and cholesteryl esters was determined (as described in Experimental Procedures) in cell pellets (A) and culture medium (B). Values are the mean ± SEM of two independent experiments.

X-XOD-induced apoptosis is inhibited by *HMGCR* gene silencing

To asses the involvement of cholesterol biosynthesis in the cell death induced by the X-XOD treatment, experiments of gene silencing of *HMGCR* with a specific shRNA cloned into an adenoviral vector (AV-sh*HMGCR*) were performed. This approach was selected because we considered gene silencing as the most specific way to inhibit a given target gene, and we selected *HMGCR* as the most rate limiting enzyme of the cholesterol biosynthesis pathway. It was observed (Supplementary Fig. S3) that the transduction of SK-N-MC cells with AV-sh*HMGCR* resulted in a 60% decrease in *HMGCR* mRNA content, and in a marked inhibition of the X-XOD-induced cell death (apoptotic cells at 48 h of treatment were 8.9 ± 2.1% in the sh*HMGCR* carrying cells compared to 25.7 ± 6.7% in the cells transduced with vehicle or with irrelevant adenovirus (sh-lamin, not shown). These results suggest that, in our cell model, the activation of cholesterol biosynthesis is deleterious for the cells, and that the cell damage produced by X-XOD can be reduced by inhibiting the cholesterol biosynthesis pathway.

HMGCR polymorphism is associated with Alzheimer's disease

The involvement of alterations in cholesterol homeostasis in AD is currently widely accepted, although to our knowledge this is the first report of such a specific induction of cholesterol biosynthesis genes in a cell model of neurodegeneration.

To determine whether our experimental model could be related to real AD, potentially functional SNPs in *HMGCR* and *HMGCS1* were selected and their association with sporadic AD investigated in two case-control samples of different geographical origin (Spain and Canada) – one including clinically diagnosed individuals, the other with a confirmed anatomo-pathological diagnosis for all individuals.

Table 2 shows the *HMGCR* SNP rs5909 was associated with AD in both samples after adjustment for the *APOE* genotype, age at onset and gender. More specifically, carrying the A allele seemed to protect from AD [the adjusted odds ratio (OR)] 0.65 in the Spanish and Canadian samples combined). As expected, ApoE4 made a much greater contribution to the risk (the adjusted OR for the carriers of the ApoE4 allele was 4.6 in the samples combined). No significant interactions were found between the rs5909 SNP and *APOE* genotype or gender: although the protective effect of the *HMGCR* A allele was greatest in the *APOE4* carrier women (OR 0.30, data not shown), no significant differences were seen with respect to other subgroups. A trend was also noted for an association of the *HMGCS1* genotype with AD risk in the test sample, although the contrast sample did not replicate this [OR for the C allele 1.18 ($P = 0.06$) and 0.86 ($P = 0.2$) in the test and contrast samples respectively]. No significant interactions were seen between *HMGCR* and *HMGCS1* polymorphisms. Previous studies have investigated the association of other SNPs in *HMGCR* and *HMGCS1* (http://www.alzgene.org) with AD. The *HMGCR* SNP rs5909 studied here was in complete linkage with the promoter SNP (rs3761740) reported by Porcellini *et al*. (2007) according to the HapMap

Table 2 *HMGCR* and *APOE* genotype distribution in two case-control AD samples

		Genotype distribution*			OR crude†		OR adjusted‡	
		HMGCR (rs5909)						
Sample		GG	GA	AA	Any A vs. GG			
Spain	Cases	489 (0.84)	95 (0.16)	2 (0.003)	0.78	(0.58–1.06)	0.69	(0.49–0.96)
	Controls	450 (0.80)	104 (0.19)	10 (0.01)		0.1		0.03
Canada	Cases	114 (0.86)	18 (0.13)	1 (0.01)	0.67	(0.35–1.28)	0.49	(0.20–1.17)
	Controls	100 (0.80)	25 (0.20)	0		0.2		0.1
Combined	Cases	603 (0.84)	113 (0.16)	3 (0.01)	0.76	(0.58–1.00)	0.65	(0.49–0.88)
	Controls	550 (0.80)	129 (0.19)	10 (0.01)		0.05		0.005
		APOE (number of APOE4 alleles)			Any 4 vs. no4			
		0	1	2				
Spain	Cases	292 (0.50)	247 (0.42)	47 (0.08)	5.6	(4.2–7.4)	5.8	(4.4–7.8)
	Controls	478 (0.85)	84 (0.15)	2 (0.003)		10^{-36}		10^{-31}
Canada	Cases	96 (0.72)	13 (0.10)	24 (0.18)	1.9	(1.04–3.5)	1.8	(0.85–3.74)
	Controls	104 (0.83)	14 (0.14)	7 (0.06)		0.03		0.1
Combined	Cases	388 (0.54)	260 (0.36)	71 (0.10)	4.6	(3.6–6.0)	4.6	(3.5–6.0)
	Controls	582 (0.85)	98 (0.14)	9 (0.01)		10^{-35}		10^{-29}

*Number of individuals with the indicated genotypes. In parentheses, frequency.
†Odds ratio with the 95% CI in parenthesis; below, the *P* value for the χ^2 test.
‡Odds ratio, 95% CI (in parentheses) and *P* value, from a logistic regression analysis that included gender, onset age, APOE and *HMGCR* genotype as the independent variables. APOE and *HMGCR* genotypes were codified into dichotomous variables: carriers (any4) and non carriers (no4) of the APOE4 allele; carriers (anyA) and non carriers (GG) of the A allele, respectively.

database. This was confirmed in the Spanish sample (data not shown). The same was true for at least another four SNPs of *HMGCR* (rs17562686, rs17238330, rs11742194 and rs10515198) in the Caucasian (CEU) population panel of the HapMap database. Thus, although the 3'UTR SNP rs5909 is predicted to affect the binding of the exonic splicing enhancers srp40 and sf2 (the A allele produces the loss of the consensus sequence according to the Pupasuite prediction algorithms (http://pupasuite.bioinfo.cipf.es/), determining the actual effect of this SNP – or of any of the other SNPs of the haplotypes – on the expression of *HMGCR* in neuronal cells requires further studies.

Discussion

While the causes of neurodegenerative diseases are still under investigation, it is clear that alterations in redox homeostasis are involved (Yankner *et al*., 2008). Although there is much evidence to relate oxidative stress and cholesterol homeostasis to AD (Koudinov *et al*., 2001; Wolozin, 2001; Panza *et al*., 2006) there is less information linking oxidative stress and aging with cholesterol biosynthesis (Cutler *et al*., 2004; Ledesma & Dotti, 2006; Martin *et al*., 2008). Neuronal loss in AD seems to be associated with increased oxidative stress (Bush, 2003; Moreira *et al*., 2005), which produces lipid peroxidation and protein and DNA oxidation (Butterfield, 2002; Butterfield & Sultana, 2007); this is attenuated by antioxidants (Montiel *et al*., 2006). Animal models and human autopsy results consistently show the accumulation of protein aggregates along with oxidative modifications of DNA, lipids and proteins (Paschen, 2003). Although oxidative stress has been linked to neurodegenerative diseases, at this point it cannot be concluded that these processes are the primary cause of neuronal death. However, it is widely accepted that they modify the progression and severity of these complex diseases.

The present data indicate that the free radical-generating X-XOD system in SK-N-MC cells induces the loss of neuronal viability in a manner dependent upon the concentration of the stressor. This agrees with the results reported by Fatokun *et al*. (2007) in a study of X-XOD in cerebellar granule neuronal cultures. Further, the present results show that cytosolic calcium, a ubiquitous intracellular messenger and regulator of cellular activity, is increased in response to the X-XOD system; in mouse pancreatic acinar cells this stress treatment also leads to increased cytosolic calcium release and calcium influx across the plasma membrane (Gonzalez *et al*., 2002).

The interplay among an increased intracellular calcium concentration, ROS formation and mitochondrial dysfunction is under examination for possible involvement in acute and chronic neurodegeneration (Chinopoulos & Adam-Vizi, 2006), although the sequence of these events prior to cell death has not yet been established. The higher levels of cytosolic calcium induced by the presence of oxidative stress suggest the activation of apoptosis.

With respect to mitochondrial dysfunction, significant quantities of cytochrome C in the cytosolic fraction were detected under oxidative stress. The time course of caspase 3 activation, PARP degradation and DNA fragmentation quantification showed that X-XOD generates a caspase-dependent apoptotic signal, indicating that diminished cell viability was due to apoptotic cell death. The cell-permeable pan-caspase inhibitor Z-VAD-fmk completely inhibited apoptosis but only partially inhibited caspase 3 activation. Thus, caspase 3 alone seems unable to initiate apoptosis. Current ideas concerning the pathways involved in caspase activation are discussed by Logue & Martin (2008).

To investigate the mechanisms involved in the apoptotic signalling induced by X-XOD in the human SK-N-MC neuroblastoma cells, microarray analysis was performed to profile the global alterations in gene expression. Interestingly, it was observed that the functional class of genes most responsive to the treatment corresponded to cholesterol and lipid metabolism. More specifically, cholesterol biosynthesis was particularly increased: virtually all the genes encoding for enzymes catalysing the production of squalene from acetoacetyl-CoA were overexpressed. Although every step of the process is important, it is generally considered that the first reactions are the most rate limiting steps. These first reactions of the pathway are catalysed by *HMGCS1* and *HMGCR*; the latter is in fact the pharmacological target of statins – cholesterol-lowering drugs that seem to have a disease modifying effect on AD (Jick *et al*., 2000).

Among the enzymes participating in cholesterol metabolism, 24-cholesterol hydroxylase (*CYP46*) – the main enzyme responsible for brain cholesterol catabolism (Lutjohann *et al*., 1996) – has been recently related to stress. Thus, it has been shown that strong oxidative stress using H_2O_2 activates its transcriptional activity two-fold (Ohyama *et al*., 2006) and that *CYP46* promotes the cholesterol loss necessary to activate survival pathways during neuronal aging (Martin *et al*., 2008). In contrast, and consistent with the induction of the cholesterol biosynthesis pathway found in our microarray analysis, we observed a reduction (2.8-fold, FDR 0.01) in the expression of *CYP46* under the mild oxidative stress conditions induced by the X-XOD system.

Interestingly, when stimuli that induce strong oxidative or reticular stress are used in this model, a downregulation of *HMGCR* and an upregulation of *CYP46* occur, respectively (unpublished results). Different kinds and intensity of stress conditions may therefore have an impact on the same target – cholesterol metabolism – but with different, perhaps even opposite, effects. Determining whether the transcriptional activation of cholesterol biosynthesis genes is a rescue or a death signal will require further studies since there is evidence suggesting that both high (Wolozin, 2001) and low (Abad-Rodriguez *et al*., 2004) cholesterol levels are harmful to neurons.

The present data suggest a strong connection exists between free radical-induced neuronal death and the deregulation of cholesterol homeostasis. After short treatment times, the mild oxidative stress induced by X-XOD leads to a reduction in cell cholesterol levels. This, in turn, induces the expression of the cholesterol biosynthesis genes (*ACSS2*, *HMGCS1*, *HMGCR*, *MVD*, *IDI1*, *FDPS*, *FDFT1*, *MVK*). The subsequent increase in cholesterol

levels may then trigger apoptosis, the first signs of which become evident in the present model after longer treatment times. Alternatively, the reduction in cholesterol levels may be the signal that induces both the apoptotic program and the cholesterol biosynthesis pathway – as a means of counteracting apoptosis; in this case, the final outcome (death/survival) would depend on the relative activity of these pathways in any given cell and situation. In this sense, the protective effect of *HMGCR* gene silencing strongly suggest that, in our cell model, mild oxidative stress associated cell death can be reduced by inhibiting cholesterol biosynthesis.

The model of cholesterol synthesis in the brain proposed by Pfrieger (2003a,b) indicates that cholesterol made in the astrocytes is loaded onto *APOE*, and this complex then exported to neurons. However, neurons are also able to synthesize cholesterol (Bjorkhem & Meaney, 2004) and although *APOE* is predominantly expressed by astrocytes, apoptosis induces neuronal *APOE* synthesis and localization in apoptotic bodies (Elliott *et al*., 2007). In agreement, the results of the present study suggest that mild free radical-induced stress upregulates the neuronal expression of *HMGCR*. *APOE* is also present in the list of upregulated genes (fold change 1.99; FDR 0.05).

To investigate whether free radical-induced cholesterol biosynthesis is associated with AD neurodegeneration, potentially functional SNPs of *HMGCR* were selected and a case-control study undertaken in two sporadic AD samples. A 3'UTR polymorphism of *HMGCR*, which is linked to other polymorphisms in this gene, including that reported by Porcellini *et al*. (2007), was found to be associated with AD, with a trend towards a stronger association in ApoE4 carrier women. For the SNP rs12514393 of *HMGCS1*, no significant association or interaction with *HMGCR* genotype was found. This result should be taken into account alongside the increasing epidemiological evidence suggesting the genetic variability of genes related to cholesterol homeostasis is an important risk factor in AD. Apart from *APOE*, over 200 polymorphic genes have been associated with AD, although how many actually contribute significantly to AD risk remains unknown (see http://www.alzgene.org and Bertram *et al*. (2007). A significant number of these genes are involved in cholesterol and lipoprotein homoeostasis (*A2M, ABCA1, APOA1, APOA4, APOC1, APOC2, APOC3, APOE, CD36, CETP, HMGCR, LDLR, LIPA, LRP1, LRP6, LPA, LPL, OLR1, SREBF1*; see http://www.polygenicpathways.co.uk and Carter (2007)). In sporadic AD, defects in cholesterol/lipoprotein function associated with these polymorphic genes (some of which are involved in the same physiological pathway as APP) may well affect – in concert with oxidative stress – APP processing and β-amyloid accumulation. In general, there is agreement that cholesterol homeostasis is somehow related to amyloid production from APP (Ledesma & Dotti, 2006).

Taken together, the results reported here identify an interesting connection between oxidative stress, apoptosis and cholesterol biosynthesis in a human neuronal cell model. They also suggest that this connection could occur in human brain neurons suffering AD-type degeneration. Ultimately, it is hoped that the mechanism of free radical-induced neuronal apoptosis may help us better understand the pathogenesis of neurodegenerative diseases.

Experimental procedures

Cell treatment and study of cell damage

Cell culture and treatment

Human neuroblastoma SK-N-MC cells were obtained from the American Type Culture Collection (HTB-10; ATCC). Xanthine was purchased from Sigma and xanthine oxidase from Roche, Madrid, Spain. Culture medium components were purchased from Gibco Laboratories. Other chemicals were purchased from Merck or Sigma. Cells were cultured in minimal essential medium (MEM) supplemented with 10% foetal bovine serum, 100 mU mL^{-1} penicillin G and 100 μg mL^{-1} streptomycin in a humidified atmosphere of 95% air and 5% CO_2. Exponentially growing stock cells at 80–90% confluency were placed in culture dishes with six multiwells (M-6), or alternatively in 96-multiwell plates (M-96), one day before stimulation. On the day of stimulation, cells were placed in fresh medium for 1 h before treatment to create the same conditions in each well. X-XOD was used at the indicated doses and times to induce oxidative stress.

Analysis of cell injury

The extent of cell injury was evaluated using the 3-(4,5-dimethylthiazol-2-yl)-2,5-diphenyl tetrazolium bromide (MTT) assay (Hansen *et al*., 1989). Briefly, the M-96 plates were seeded at a rate of 30 000 cells/well and, after exposure to X-XOD, incubated with 0.5 mg mL^{-1} MTT for 3 h at 37 °C. The MTT/formazan released from the cells during overnight incubation at 37 °C with 100 μL extraction buffer [20% sodium dodecyl sulphate (SDS), 50% formamide adjusted to pH 4.7 with 0.02% acetic acid and 0.025 N HCl] was determined. Optical densities were measured at 570 nm using an automated Model 680 (Bio-Rad) microplate reader.

Intracellular calcium content quantification

SK-N-MC cells seeded onto M-96 plates were incubated with the membrane-permeable Ca^{2+}-sensitive dye fluo-4-AM (10 μM) in culture medium for 1 h at 37 °C. They were then washed twice in Tyrode-Hepes solution (145 mM NaCl, 2.7 mM KCl, 1.0 mM $MgCl_2$, 1.8 mM $CaCl_2$, 10 mM glucose and 10 mM Hepes; pH 7.4) with probenecid (1 mM) and incubated for 15 min at room temperature (RT) in the dark. Changes in fluorescence (excitation 485 nm, emission 550 nm) were measured using a Fluostar fluorescent plate reader (BMG Labtechnologies, Offenburg, Germany). Baseline levels of fluorescence were monitored for 30 s before applying the treatment using an automatic dispenser. After stimulation, changes in fluorescence were monitored every 10 s over a period of 120 s. For normalizing the fluo-4-AM signals, responses from each well were calibrated by determining the maximum and minimum fluorescence values. At the end of each experiment, 0.5% Triton X-100 (F_{max}) was

added, followed by 106 mM $MnCl_2$ (F_{min}). The results are presented as percentages of F_{max}-$F_{min.}$

Cytochrome c release

The subcellular distribution of cytochrome *c* was analysed by immunocytochemistry. Briefly, after the treatments, cells grown on coverslips at a density of 100 000 cells/well in a 24-well plate were fixed with 4% paraformaldehyde in PBS at room temperature for 20 min and permeabilized with PBS containing 0.2% Triton X-100 and 2% horse serum at 4 °C overnight. They were then incubated at RT for 1 h with anti-cytochrome *c* (Pharmingen, Madrid, Spain) before further incubation at RT for 1 h with Alexa 488 anti-mouse immunoglobulin G (Invitrogen, CA, USA). For nucleus staining, coverslips were incubated in PBS containing 5 μg mL^{-1} DAPI (Sigma, Madrid, Spain) for 15 min. Reactive images were observed by fluorescence microscopy suing a BX 51 apparatus (Olympus, Hamburg, Germany).

To determine the localization of cytochrome C, living cells were incubated with 2 μM MitoTracker® Red (Molecular Probes) for 45 min at 37 °C and rinsed with pre-warmed PBS. MitoTracker-loaded cells were fixed in 4% paraformaldehyde in PBS at RT for 10 min, and then in 100% methanol at –20 °C for 10 min, washed, and then used for immunofluorescence as indicated above. Fluorescence was analysed using a Bio-Rad confocal microradiance microscope.

Cleaved caspase 3 labelling

Cleaved caspase 3 labelling was performed following the modified method of Belloc *et al*. (2000). Cells incubated under the different treatments with or without 50 μM caspase inhibitor Z-VAD-fmk were pelleted and resuspended in 200 μL of buffer stain (0.01% NaN_3, 0.2% saponin and 5% BSA in PBS) and incubated for 15 min at RT. The suspension was then centrifuged and labelling performed by adding 50 μL of buffer stain containing 2 μL of polyclonal phycoerythrin (PE)-conjugated anti-active caspase 3 antibodies (BD Biosciences-Pharmingen, Madrid, Spain) and incubating for 20 min at 4 °C. The samples were washed twice with buffer stain and analysed by flow cytometry (FACSCalibur).

PARP p85 fragment

The PARP p85 fragment concentration was evaluated by Western blotting. At the end of experiments, cells were washed in cold PBS and lysed in Laemmli's SDS sample buffer before loading onto 10% SDS–polyacrylamide gels. Protein bands were transferred to nitrocellulose membranes (Bio-Rad). These were further processed by incubating with the primary anti-PARP p85 fragment antibody (Promega, Madrid, Spain) for 2 h at RT. This was followed by incubation with a secondary antibody [anti-rabbit/goat (Nordic) horseradish peroxidase conjugate]. Visualization of the bands was performed using the enhanced chemiluminescence Western blotting analysis system (Pharmacia Biotech, Barcelona, Spain). As an internal control, α-tubulin levels were examined [via the reaction with anti-α-tubulin (Sigma)] in the same blot at the same time.

Quantification of apoptosis by flow cytometry

Apoptosis was determined by propidium iodide (PI) staining and fluorescence-activated cell sorting analysis. Briefly, after treatment, cells that remained attached to the M-6 plates were harvested in PBS and stained in a buffer (0.1% sodium citrate, 0.3% NP-40 and 0.02 mg mL^{-1} RNase A) containing 50 μg mL^{-1} propidium iodide. Samples were analysed by flow cytometry (FACSCalibur) using Cell Quest software (Becton–Dickinson, Madrid, Spain). Apoptosis was measured as the percentage of cells with a sub G1 phase DNA content in the propidium iodide intensity-area histogram plot.

Determination of cholesterol synthesis

The synthesis of cholesterol was determined by measuring the incorporation of radioactive acetate into free and esterified cellular cholesterol. SK-N-MC cells were treated with X-XOD (10 μM xanthine/50 mU mL^{-1} xanthine oxidase), and [1–^{14}C] acetate (3.4 mM, 60 Ci mol^{-1}) was added 6 h before the end of each incubation period. Cholesterol biosynthetic activity was estimated according to the incorporation of the radiolabel into the cholesterol. After treatment, the medium was collected and the cells washed twice with ice-cold PBS before being harvested by scraping them into PBS. Cell protein content was determined in the cell homogenates using the Bradford method. The quantity of cells equivalent to 1 mg of protein was assayed as follows. Lipids were extracted from the medium and cells following procedure of Bligh & Dyer (1959). Free and esterified cholesterol molecules were separated by thin-layer chromatography using an n-hexane/ethyl ether/acetic acid (80/20/1, v/v/v) solvent. The spots were rendered visible by exposure to iodine vapour. Radiometric measurements of lipid spots were made in a liquid scintillation counter.

Analysis of differential gene expression using microarrays

The Applied Biosystems Human Genome Survey Microarray (P/N 4337467), which contains 31 700 60-mer oligonucleotide probes representing 29 098 individual human genes, was used to analyse gene expression profiles in SK-N-MC cells cultured for 18 h in the absence (vehicle-treated control; $n = 6$) or presence of X-XOD (10 μM xanthine/50 mU mL^{-1} xanthine oxidase; $n = 6$). Total RNA was extracted using the High Pure RNA Isolation kit (Roche), and the RNA quality assessed in an Agilent 2100 Bioanalyzer (Agilent, Madrid, Spain). Digoxigenin-UTP labelled cRNA was generated and amplified from 1 μg of total RNA from each sample using the Applied Biosystems Chemiluminescent RT-IVT Labeling Kit v 1.0 (P/N 4340472) according to the manufacturer's protocol (P/N 4339629). Array hybridization was performed for 16 h at 55 °C. Chemiluminescence detection, image acquisition and analysis were performed using the Applied Biosystems Chemiluminescence Detection Kit (P/N 4342142) and Applied Biosystems 1700 Chemiluminescent Microarray Analyzer (P/N 4338036) following the manufacturer's protocols (P/N 4339629). Images were auto-gridded and the

chemiluminescent signals quantified, the background subtracted, and then spot and spatially normalized using Applied Biosystems 1700 Chemiluminescent Microarray Analyzer software v 1.1 (P/N 4336391). The detection threshold was set at a signal to noise ratio (S/N) of > 0. A quality flag of < 5000 was chosen. Detection was deemed positive if the appropriate signal was seen in three replicates.

Data analysis

Data from all samples were subjected to quantile normalization (Bolstad *et al*., 2003) and the expression profiles for probes corresponding to replicated genes were averaged. Differential expression analysis for treated and control cells was performed using the rank product method (Breitling *et al*., 2004). A permutation-based estimation procedure with 100 random iterations was then used to estimate the false discovery rate (FDR) value. Biological functions associated with differentially expressed genes were obtained by examining the Gene Ontology (GO) Biological Processes that were enriched in the list of genes. This was undertaken employing GENECODIS software (Carmona-Saez *et al*., 2007), which use the hypergeometric distribution to discover enrichment of GO annotations in a list of genes. Correction for multiple hypothesis testing was conducted using the FDR method of Benjamini & Hochberg (1995).

Quantitative RT-PCR

The mRNA transcribed from each gene was quantified by two-step reverse transcription (RT)-PCR using TaqMan low density arrays (Applied Biosystems, Madrid, Spain) as previously described (Ramos *et al*., 2006). Briefly, total RNA isolated with Tripure (Boehringer) from SK-N-MC cells was subjected (1 μg RNA in 100 μL reaction volume) to reverse transcription using the High Capacity cDNA Archive Kit (Applied Biosystems). Real-time PCR was then performed in TaqMan arrays – cDNA was mixed with TaqMan Universal PCR Master Mix NoAmpEraseUNG (Applied Biosystems) and applied to the arrays (5 μL of the RT reaction in 100 μL reaction volumes per port). PCR (94.5 °C for 10 min plus 40 cycles of 97 °C for 30 s and 59.7 °C for 1 min) was performed in an ABI 7900HT apparatus (Applied Biosystems). The relative quantities in treated and untreated cells were determined by the $\Delta\Delta C_t$ method using SDS v2.1.1 software; *GAPDH* was used as the housekeeping gene, the expression of which did not change at any time.

Generation of adenoviral vectors and gene silencing assays

Vectors that express sh*HMGCR* under the control of U6 promoter were constructed by inserting pairs of annealed DNA oligonucleotides into the linearized pENTR™/U6 vector (Invitrogen™). U6-driven sh*HMGCR* cassette in pENTR™/U6 donor vector was transferred into the adenoviral acceptor vector pAd/BLOCK-iT™-DEST to generate the pAd-sh*HMGCR*, according to the protocol of the manufacturer using the BLOCK-iT™. adenoviral RNAi expression system (Invitrogen™). Low-passage HEK 293A cells were then transfected with pAd-sh*HMGCR* and supernatants containing adenoviruses expressing sh*HMGCR* (Ad-sh*HMGCR*) were amplified by infecting larger scale of HEK293 cells. Adenoviral titres were determined by plaque assays using HEK 293A cell line. An adenovirus expressing a shRNA to lamin A/C (Ad-shlamin), included in the BLOCK-iT™ adenoviral RNAi expression system, was used as a negative control (REF). For gene silencing assays, SK-N-MC cells were transduced with adenovirus expressing shRNA at a moi of 15 during 18 h 72 h after transduction, cells were treated with X-XOD as previously described. RNA was extracted for the examination of gene knockdown by (RT)-QPCR.

Genetic association

Study subjects

The test sample consisted of 586 patients with sporadic AD (mean age at onset 73.1 ± 8.8 years; 67% females) and 564 controls (age at examination 71.3 ± 13.6 years; 57% females) from the same regions, recruited at the neurology departments of the participating hospitals. The patients had a diagnosis of probable AD according to the NINCDS-ADRDA (McKhann *et al*., 1984) or DSM-IV (Wilson & Skodol, 1994) criteria for Alzheimer's dementia. The cognitive status of the controls was measured using the Mini Mental, MEC and WAIS Cubes tests. This clinically diagnosed AD sample is the sum of two Spanish samples recruited independently, that were collapsed after showing that the diagnostic criteria and the distribution of the studied and other polymorphisms (Ramos *et al*., 2006) were not significantly different. All subjects gave their informed consent to be included in the study, which was approved by the Ethics Committees of the participating institutions.

A Canadian case-control sample (contrast) was composed of 133 patients with AD (mean age at onset 69.3 ± 9.7 years; mean ± SD; 57% females) and 125 controls (mean age at examination 73.9 ± 7.0 years; 50% females). All these subjects underwent autopsy at the London Health Sciences Centre, University of Western Ontario. The criteria for AD included a diagnosis of dementia by a neurologist and an NIA/Reagan score showing a high probability that dementia was due to AD. The criteria for controls were documented normal mental status (not necessarily recorded by a neurologist) on clinical exam prior to death, and an NIA/Reagan score showing a low probability of AD (Anon, 1997).

Genotyping and statistics

HMGCR 3'UTR (dbSNP code rs5909) and promoter (rs3761740) polymorphisms, and the *HMGCS1* 5'UTR polymorphism (rs12514393), were analysed using predesigned TaqMan-MGB® Assays (Applied Biosystems) (C__11432463_10, C__27476930_10 and C___1878502_10, respectively) following the manufacturer's instructions. All the subjects had previously been genotyped for *APOE* (Ramos *et al*., 2006; Bullido *et al*., 2007).

Genotypes and allele distributions were compared using the χ^2 test (crude analysis) and in logistic regression models adjusting for age at AD onset, gender and sample origin (adjusted analysis). The association between the genotypes and AD was expressed as the odds ratio (OR) with 95% confidence intervals (CIs). SPSS v.15.0 software was used for all statistical analyses.

Acknowledgments

This work was supported by the *Ministerio de Educación y Ciencia* (GEN2003-20235-C05-05), the *Obra Social Caja Madrid*, the *Comunidad Autónoma de Madrid* (GR/SAL/0783/e2004), the I.M.S.E.R.S.O and the *Ministerio de Sanidad y Consumo* (*Instituto de Salud Carlos III*). The institutional grant awarded by the *Fundación Ramón Areces* to the *Centro de Biología Molecular Severo Ochoa* is gratefully acknowledged. We thank Dr L. Ledesma for critical reading of the manuscript. We thank Prof A. García and Dr M. García for their cooperation in the calcium experiments, and Drs P. Gil, P. Coria, M. Rosich-Estragó, A. Labad-Alquézar and D. Muñoz for their cooperation in the generation of the case-control samples. We are grateful to the *Asociación de Familiares de Alzheimer de Madrid (AFAL)* for continuous encouragement and help. This work was made possible by the generous participation of the patients, the control subjects and their families.

References

Abad-Rodriguez J, Ledesma MD, Craessaerts K, Perga S, Medina M, Delacourte A, Dingwall C, De Strooper B, Dotti CG (2004) Neuronal membrane cholesterol loss enhances amyloid peptide generation. *J. Cell Biol*. **167**, 953–960.

Andersen JK (2004) Iron dysregulation and Parkinson's disease. *J. Alzheimers. Dis*. **6**, S47–S52.

Anon. (1997) Consensus recommendations for the postmortem diagnosis of Alzheimer's disease. The National Institute on Aging, and Reagan Institute Working Group on Diagnostic Criteria for the Neuropathological Assessment of Alzheimer's Disease. *Neurobiol. Aging*. **18**, S1–S2.

Belloc F, Belaud-Rotureau MA, Lavignolle V, Bascans E, Braz-Pereira E, Durrieu F, Lacombe F (2000) Flow cytometry detection of caspase 3 activation in preapoptotic leukemic cells. *Cytometry* **40**, 151–160.

Benjamini Y, Hochberg Y (1995) Controlling the false discovery rate: a practical and powerful approach to multiple testing. *J. R. Stat Soc. Series B*. **57**, 289–300.

Bertram L, McQueen MB, Mullin K, Blacker D, Tanzi RE (2007) Systematic meta-analyses of Alzheimer disease genetic association studies: the AlzGene database. *Nat. Genet*. **39**, 17–23.

Bjorkhem I, Meaney S (2004) Brain cholesterol: long secret life behind a barrier. *Arterioscler Thromb. Vasc Biol*. **24**, 806–815.

Blalock EM, Geddes JW, Chen KC, Porter NM, Markesbery WR, Landfield PW (2004) Incipient Alzheimer's disease: microarray correlation analyses reveal major transcriptional and tumor suppressor responses. *Proc. Natl. Acad. Sci. USA* **101**, 2173–2178.

Bligh EG, Dyer WJ (1959) A rapid method of total lipid extraction and purification. *Can. J. Biochem. Physiol*. **37**, 911–917.

Bolstad BM, Irizarry RA, Astrand M, Speed TP (2003) A comparison of normalization methods for high density oligonucleotide array data based on variance and bias. *Bioinformatics*. **19**, 185–193.

Breitling R, Armengaud P, Amtmann A, Herzyk P (2004) Rank products: a simple, yet powerful, new method to detect differentially regulated genes in replicated microarray experiments. *FEBS Lett*. **573**, 83–92.

Bullido MJ, Martinez-Garcia A, Artiga MJ, Aldudo J, Sastre I, Gil P, Coria F, Munoz DG, Hachinski V, Frank A, Valdivieso F (2007) A TAP2 genotype associated with Alzheimer's disease in APOE4 carriers. *Neurobiol. Aging*. **28**, 519–523.

Bush AI (2003) The metallobiology of Alzheimer's disease. *Trends Neurosci*. **26**, 207–214.

Butterfield DA (2002) Amyloid beta-peptide (1-42)-induced oxidative stress and neurotoxicity: implications for neurodegeneration in Alzheimer's disease brain. A review. *Free Radic Res*. **36**, 1307–1313.

Butterfield DA, Sultana R (2007) Redox proteomics identification of oxidatively modified brain proteins in Alzheimer's disease and mild cognitive impairment: insights into the progression of this dementing disorder. *J. Alzheimers. Dis*. **12**, 61–72.

Carmona-Saez P, Chagoyen M, Tirado F, Carazo JM, Pascual-Montano A (2007) GENECODIS: a web-based tool for finding significant concurrent annotations in gene lists. *Genome. Biol*. **8**, R3.

Carter CJ (2007) Convergence of genes implicated in Alzheimer's disease on the cerebral cholesterol shuttle: APP, cholesterol, lipoproteins, and atherosclerosis. *Neurochem. Int*. **50**, 12–38.

Chinopoulos C, Adam-Vizi V (2006) Calcium, mitochondria and oxidative stress in neuronal pathology. Novel aspects of an enduring theme. *FEBS J*. **273**, 433–450.

Cutler RG, Kelly J, Storie K, Pedersen WA, Tammara A, Hatanpaa K, Troncoso JC, Mattson MP (2004) Involvement of oxidative stress-induced abnormalities in ceramide and cholesterol metabolism in brain aging and Alzheimer's disease. *Proc. Natl. Acad. Sci. USA* **101**, 2070–2075.

Elliott DA, Kim WS, Jans DA, Garner B (2007) Apoptosis induces neuronal apolipoprotein-E synthesis and localization in apoptotic bodies. *Neurosci. Lett*. **416**, 206–210.

Fatokun AA, Stone TW, Smith RA (2007) Hydrogen peroxide mediates damage by xanthine and xanthine oxidase in cerebellar granule neuronal cultures. *Neurosci. Lett*. **416**, 34–38.

Forman MS, Lee VM, Trojanowski JQ (2003) 'Unfolding' pathways in neurodegenerative disease. *Trends Neurosci*. **26**, 407–410.

Ghosh A, Greenberg ME (1995) Calcium signaling in neurons: molecular mechanisms and cellular consequences. *Science (New York, N.Y.)* **268**, 239–247.

Gibson GE, Huang HM (2005) Oxidative stress in Alzheimer's disease. *Neurobiol. Aging*. **26**, 575–578.

Gomez-Isla T, West HL, Rebeck GW, Harr SD, Growdon JH, Locascio JJ, Perls TT, Lipsitz LA, Hyman BT (1996) Clinical and pathological correlates of apolipoprotein E epsilon 4 in Alzheimer's disease. *Ann. Neurol*. **39**, 62–70.

Gonzalez A, Schmid A, Salido GM, Camello PJ, Pariente JA (2002) XOD-catalyzed ROS generation mobilizes calcium from intracellular stores in mouse pancreatic acinar cells. *Cell Signal*. **14**, 153–159.

Hajnoczky G, Davies E, Madesh M (2003) Calcium signaling and apoptosis. *Biochem. Biophys. Res. Commun*. **304**, 445–454.

Hansen MB, Nielsen SE, Berg K (1989) Re-examination and further development of a precise and rapid dye method for measuring cell growth/cell kill. *J. Immunol. Methods* **119**, 203–210.

Harman D (1981) The aging process. *Proc. Natl. Acad. Sci. USA* **78**, 7124–7128.

Hayes JD, Ellis EM, Neal GE, Harrison DJ, Manson MM (1999) Cellular response to cancer chemopreventive agents: contribution of the antioxidant responsive element to the adaptive response to oxidative and chemical stress. *Biochem. Soc. Symp*. **64**, 141–168.

Hengartner MO (2000) The biochemistry of apoptosis. *Nature* **407**, 770–776.

Jarvik GP, Austin MA, Fabsitz RR, Auwerx J, Reed T, Christian JC, Deeb S (1994) Genetic influences on age-related change in total cholesterol, low density lipoprotein-cholesterol, and triglyceride levels: longitudinal apolipoprotein E genotype effects. *Genet. Epidemiol*. **11**, 375–384.

Jick H, Zornberg GL, Jick SS, Seshadri S, Drachman DA (2000) Statins and the risk of dementia. *Lancet* **356**, 1627–1631.

Koudinov AR, Berezov TT, Koudinova NV (2001) The levels of soluble amyloid beta in different high density lipoprotein subfractions distinguish Alzheimer's and normal aging cerebrospinal fluid: implication for brain cholesterol pathology? *Neurosci. Lett*. **314**, 115–118.

Ledesma MD, Dotti CG (2006) Amyloid excess in Alzheimer's disease: what is cholesterol to be blamed for? *FEBS Lett*. **580**, 5525–5532.

Lee HG, Zhu X, Castellani RJ, Nunomura A, Perry G, Smith MA (2007) Amyloid-beta in Alzheimer disease: the null versus the alternate hypotheses. *J. Pharmacol. Exp. Ther*. **321**, 823–829.

Logue SE, Martin SJ (2008) Caspase activation cascades in apoptosis. *Biochem. Soc. Trans*. **36**, 1–9.

Lutjohann D, Breuer O, Ahlborg G, Nennesmo I, Siden A, Diczfalusy U, Bjorkhem I (1996) Cholesterol homeostasis in human brain: evidence for an age-dependent flux of 24S-hydroxycholesterol from the brain into the circulation. *Proc. Natl. Acad. Sci. USA* **93**, 9799–9804.

Malhotra JD, Kaufman RJ (2007) The endoplasmic reticulum and the unfolded protein response. *Semin. Cell Dev. Biol*. **18**, 716–731.

Marques CA, Keil U, Bonert A, Steiner B, Haass C, Muller WE, Eckert A (2003) Neurotoxic mechanisms caused by the Alzheimer's disease-linked Swedish amyloid precursor protein mutation: oxidative stress, caspases, and the JNK pathway. *J. Biol. Chem*. **278**, 28294–28302.

Martin MG, Perga S, Trovo L, Rasola A, Holm P, Rantamaki T, Harkany T, Castren E, Chiara F, Dotti CG (2008) Cholesterol Loss Enhances TrkB Signaling in Hippocampal Neurons Aging *in Vitro*. *Mol. Biol. Cell* **19**, 2101–2112.

McKhann G, Drachman D, Folstein M, Katzman R, Price D, Stadlan EM (1984) Clinical Diagnosis of Alzheimer's Disease: report of the NINCDS-ADRDA Work Group under the auspices of Department of Health and Human Services Task Force on Alzheimer's Disease. *Neurology*. **34**, 939–944.

Montiel T, Quiroz-Baez R, Massieu L, Arias C (2006) Role of oxidative stress on beta-amyloid neurotoxicity elicited during impairment of energy metabolism in the hippocampus: protection by antioxidants. *Exp. Neurol*. **200**, 496–508.

Moreira PI, Siedlak SL, Aliev G, Zhu X, Cash AD, Smith MA, Perry G (2005) Oxidative stress mechanisms and potential therapeutics in Alzheimer disease. *J. Neural. Transm*. **112**, 921–932.

Nunomura A, Perry G, Pappolla MA, Wade R, Hirai K, Chiba S, Smith MA (1999) RNA oxidation is a prominent feature of vulnerable neurons in Alzheimer's disease. *J. Neurosci*. **19**, 1959–1964.

Nunomura A, Perry G, Aliev G, Hirai K, Takeda A, Balraj EK, Jones PK, Ghanbari H, Wataya T, Shimohama S, Chiba S, Atwood CS, Petersen RB, Smith MA (2001) Oxidative damage is the earliest event in Alzheimer disease. *J. Neuropathol. Exp. Neurol*. **60**, 759–767.

Nunomura A, Castellani RJ, Zhu X, Moreira PI, Perry G, Smith MA (2006) Involvement of oxidative stress in Alzheimer disease. *J. Neuropathol. Exp. Neurol*. **65**, 631–641.

Ohyama Y, Meaney S, Heverin M, Ekstrom L, Brafman A, Shafir M, Andersson U, Olin M, Eggertsen G, Diczfalusy U, Feinstein E, Bjorkhem I (2006) Studies on the transcriptional regulation of cholesterol 24-hydroxylase (CYP46A1): marked insensitivity toward different regulatory axes. *J. Biol. Chem*. **281**, 3810–3820.

Panza F, D'Introno A, Colacicco AM, Capurso C, Pichichero G, Capurso SA, Capurso A, Solfrizzi V (2006) Lipid metabolism in cognitive decline and dementia. *Brain Res. Rev*. **51**, 275–292.

Paschen W (2003) Endoplasmic reticulum: a primary target in various acute disorders and degenerative diseases of the brain. *Cell Calcium*. **34**, 365–383.

Pfrieger FW (2003a) Cholesterol homeostasis and function in neurons of the central nervous system. *Cell. Mol. Life Sci*. **60**, 1158–1171.

Pfrieger FW (2003b) Outsourcing in the brain: do neurons depend on cholesterol delivery by astrocytes? *Bioessays*. **25**, 72–78.

Porcellini E, Calabrese E, Guerini F, Govoni M, Chiappelli M, Tumini E, Morgan K, Chappell S, Kalsheker N, Franceschi M, Licastro F (2007) The hydroxy-methyl-glutaryl CoA reductase promoter polymorphism is associated with Alzheimer's risk and cognitive deterioration. *Neurosci. Lett*. **416**, 66–70.

Ramos MC, Tenorio R, Martinez-Garcia A, Sastre I, Vilella-Cuadrada E, Frank A, Rosich-Estrago M, Valdivieso F, Bullido MJ (2006) Association of DSC1, a gene modulated by adrenergic stimulation, with Alzheimer's disease. *Neurosci. Lett*. **408**, 203–208.

Rubinsztein DC, Easton DF (1999) Apolipoprotein E genetic variation and Alzheimer's disease: a meta-analysis. *Dement. Geriatr. Cogn. Disord*. **10**, 199–209.

Stadtman ER (2002) Importance of individuality in oxidative stress and aging. *Free Radic Biol. Med*. **33**, 597–604.

Tan ZS, Seshadri S, Beiser A, Wilson PW, Kiel DP, Tocco M, D'Agostino RB, Wolf PA (2003) Plasma total cholesterol level as a risk factor for Alzheimer disease: the Framingham Study. *Arch. Intern. Med*. **163**, 1053–1057.

White AR, Zheng H, Galatis D, Maher F, Hesse L, Multhaup G, Beyreuther K, Masters CL, Cappai R (1998) Survival of cultured neurons from amyloid precursor protein knock-out mice against Alzheimer's amyloid-beta toxicity and oxidative stress. *J. Neurosci*. **18**, 6207–6217.

Wilson HS, Skodol A (1994) Special report: DSM-IV: overview and examination of major changes. *Arch. Psychiatr. Nurs*. **8**, 340–347.

Wirths O, Thelen K, Breyhan H, Luzon-Toro B, Hoffmann KH, Falkai P, Lutjohann D, Bayer TA (2006) Decreased plasma cholesterol levels during aging in transgenic mouse models of Alzheimer's disease. *Exp. Gerontol*. **41**, 220–224.

Wolozin B (2001) A fluid connection: cholesterol and Abeta. *Proc. Natl. Acad. Sci. USA* **98**, 5371–5373.

Yankner BA, Lu T, Loerch P (2008) The aging brain. *Annu. Rev. Pathol*. **3**, 41–66.

Supporting Information

Additional Supporting Information may be found in the online version of this article:

Fig. **S1** Cell injury and cytosolic calcium levels after oxidative stress.

(A) Cells subjected to 18 h of treatment with 10 μM xanthine (X) and the indicated concentrations of xanthine oxidase (XOD) were analysed for injury using the MTT reduction assay. Values are expressed relative to the optical density of untreated control cells at 570 nm. Each value represents the average of three replicates ± the standard error (***$P < 0.001$, **$P < 0.01$ and *$P < 0.05$ compared to controls [Student *t*-test]). (B) Elevation of intracellular calcium levels after oxidative stress. Cells loaded with fluo-4 AM were stimulated with 10 μM xanthine (X)-xanthine oxidase (XOD) at the indicated concentrations. Changes in fluorescence were monitored over 120 s. Data are expressed as the percentage F_{max}–F_{min} (mean ± SEM) of at least four

independent experiments. The Student *t*-test ($P < 0.001$) revealed significant differences between the results for the treated cells and the controls.

Fig. S2 X-XOD upregulated genes in neuroblastoma cells.

The mRNA transcribed from each gene was quantified by RT-QPCR (see Experimental procedures) in SK-N-MC cells after 12, 18 and 24 h of X-XOD treatment, and normalized in terms of the *GAPDH* mRNA level. The relative quantity with respect to control cultures (mean ± standard error) is shown. The horizontal line at 1 is the baseline.

Fig. S3 Effect of *HMGCR* gene silencing on X-XOD induced apoptosis.

(A) Relative mRNA content of *HMGCR*, quantified by RT-QPCR and normalized in terms of the *GAPDH* mRNA level in SK-N-MC cells transduced for 72 h with adenovirus carrying sh*HMGCR* or with vehicle (mock transduced) (see Experimental procedures. (B) Quantification of apoptotic death in the cells treated with X-XOD (black bars) or untreated (white bars) for 48 h. Apoptosis was assessed by propidium iodide staining and analysed by flow cytometry. Results are the mean ± SEM of three independent experiments. Student *t*-test significance for the cell death in X-XOD treated cells compared to control cells ($*P < 0.05$) or to sh*HMGCR* transduced/X-XOD treated cells ($\#P < 0.05$).

Supplementary Table Complete list of the genes showing a significant change in expression modulated by X-XOD (FDR < 0.05)

Please note: Wiley-Blackwell are not responsible for the content or functionality of any supporting materials supplied by the authors. Any queries (other than missing material) should be directed to the corresponding author for the article.